Proceedings of the 2009 IEEE International Conference on Systems, Man, and Cybernetics
San Antonio, TX, USA - October 2009

Computational Modeling of Risk-Dependent Eye Movements of Car Drivers

Takashi Omori
College of Engineering
Tamagawa University
Tokyo, Japan
omori@lab.tamagawa.ac.jp

Masayoshi Sato, Koichiro Yamauchi
Graduate School of Information Science and Technology
Hokkaido University
Sapporo, Japan
{justice, yamauchi}@complex.eng.hokudai.ac.jp

Satoru Ishikawa
Department of Psychology and Applied Communication
Hokusei Gakuen University
Sapporo, Japan
ishi_s@hokusei.ac.jp

Toshihiro Wakita
Toyota Central R&D Labs., Inc.
Nagakute, Japan
wakita@mosk.tytlabs.co.jp

***Abstract*—In this study, we present a computational model of a car driver's cognitive process and eye movement in relation to risk evaluation for greater safe driving assistance. The model status is mainly determined by visual inputs. In simulations, we reconstructed and predicted the driver eye movements while driving using an environmental risk calculation model, and compared them to the eye movements of an actual human driver.**

***Keywords*—risk evaluation, eye-movement, car driving, cognitive process, computational modeling**

I. INTRODUCTION

Many kinds of driving assistance systems are being developed as part of an intelligent transport systems (ITS) for improving automobile safety. To effectively make driving safer, it is important that the system assist drivers based on their own cognitive processes [1][2][3]. To achieve this, we need a model of the human cognitive process for driving an automobile. Even though many of models for human driving behaviors have been proposed [4][5][6], no single model has been able to duplicate all human driving situations because directly measuring the cognitive processes involved is impossible.

We approach this problem by focusing on eye movement, which constitutes a major part of information gathering while driving a car, and established a cognitive model of a driver based on eye movements while driving [3]. In a previous study [7], we proposed a cognitive model for driver eye movement based on risk evaluation, and reconstructed the actual eye movements of drivers. In this study, we improved the model especially to predict the eye movements of drivers entering intersections with blind sides and evaluated the model by comparing them to actual drivers eye movements while he was driving the road simulated.

II. COMPUTATIONAL MODELING OF EYE MOVEMENT

We present a broad overview of the proposed model in Fig. 1. First, the visual perception system builds a distribution calculation system based on the images viewed. The distribution calculation system estimates the probability distributions of visible and non-visible objects. The driver acquires a probability distribution of the visible objects for the visible area such as pedestrians and oncoming cars based on the laws of physics and a probability distribution of the non-visible mobile objects for the non-visible areas such as blind intersections and behind the obstacles.

Then the driver detects risk by estimating the overlapping area between one of these two distributions and a probability distribution of his own car's position based on the driver's intention. We call these overlapping areas the predicted visible risky area (PVRA) and the predicted non-visible risky area (PNRA), respectively (Fig. 2).

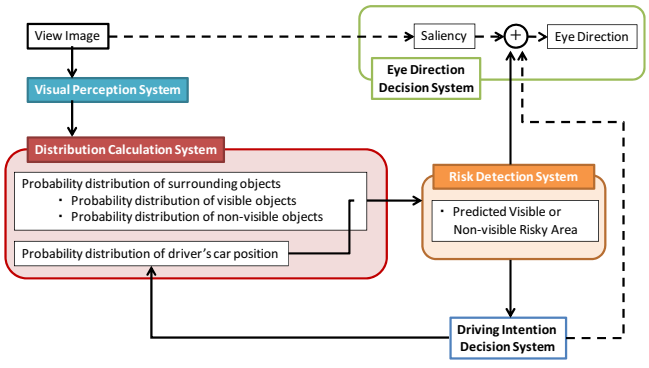

Figure 1. Overview of the proposed model

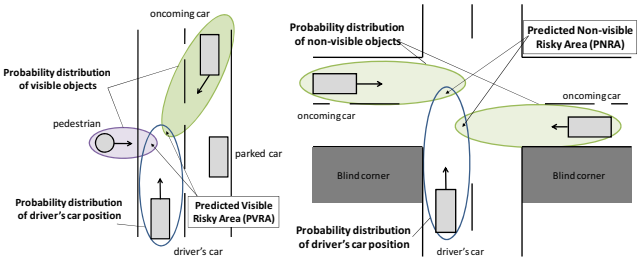

Figure 2. PVRA (left) and PNRA (right)

The driver tries to see the high risky areas to predict the precise course of any approaching visible or non-visible objects [8]. As a result of this observation, he changes his course to avoid an accident if he judges it to be dangerous.

In Sections II.A. and II.B., we explain in detail the probability distributions of visible and non-visible objects.

A. Model of the Visible Risky Area

1) Distribution prediction of the visible objects:

To calculate PVRA, the position of visible objects several seconds in the future is predicted using a Kalman filter [9]. The predicted position is represented by a normal distribution called a probability distribution of visual objects.

Moreover, several sets of such position predictors are used to allow for various possible approaching courses of the objects. In this study, we simultaneously used three Kalman filters: *go-straight*, *right-turn*, and *left-turn*. The weighted sum of these three predicted distributions was used to calculate an object's predicted distribution. The variance of each normal distribution accounts for the prediction ambiguity. The weights for the three distributions were determined by the error between each predicted position and the visible object's actual position.

For example, the *go-straight* Kalman filter is expressed as below:

$$\mathbf{K}_{forward}(t) \leftarrow \hat{\Sigma}_{forward}(t)\left(\hat{\Sigma}_{forward}(t)+\Sigma_v\right)^{-1} \quad (1)$$

$$\hat{\mathbf{x}}_{forward}(t) \leftarrow \hat{\mathbf{x}}_{forward}(t)+\mathbf{K}_{forward}(t)\left\{y(t)-\hat{\mathbf{x}}_{forward}(t)\right\} \quad (2)$$

$$\hat{\Sigma}_{forward}(t) \leftarrow \hat{\Sigma}_{forward}(t)-\mathbf{K}_{forward}(t)\hat{\Sigma}_{forward}(t) \quad (3)$$

$$\hat{\mathbf{x}}_{forward}(t+1) \leftarrow \mathbf{F}_{forward}\hat{\mathbf{x}}_{forward}(t) \quad (4)$$

$$\hat{\Sigma}_{forward}(t+1) \leftarrow \mathbf{F}_{forward}\hat{\Sigma}_{forward}(t)\mathbf{F}_{forward}{}^{T}+\mathbf{G}\Sigma_w\mathbf{G}^T \quad (5)$$

where $\hat{\mathbf{x}}_{forward}(t), \mathbf{y}(t), \mathbf{K}_{forward}(t)$ denote the inner state of the object's velocity and position, observed target information, and the Kalman gain at time *t*, respectively. ***G*** denotes white noise, and $\boldsymbol{F}_{forward}$ and $\hat{\Sigma}_{forward}(t)$ denote the state transition matrix and error covariance matrix of the *go-straight* Kalman filter.

The Kalman gain is updated by (1). The internal state and the error covariance matrix of the *go-straight* Kalman filter are updated using observed target information $\mathbf{y}(t)$ by (2) and (3), respectively. Furthermore, the inner state of the object's velocity and position and the error covariance matrix at time *t+1* are predicted by (4) and (5), respectively.

Using these equations, we predict the object's position distribution for each time step to N futurer steps and express it as (6).

$$p_{t+n}(x) = w_{forward}\aleph\left(\hat{\mathbf{x}}_{forward}(t+n), \hat{\Sigma}_{forward}(t+n)\right)+ w_{left}\aleph\left(\hat{\mathbf{x}}_{left}(t+n), \hat{\Sigma}_{left}(t+n)\right)+ w_{right}\aleph\left(\hat{\mathbf{x}}_{right}(t+n), \hat{\Sigma}_{right}(t+n)\right) \quad (6)$$

where $\aleph(\mathbf{u},\Sigma)$ denotes a normal distribution with average $\aleph(\mathbf{u},\Sigma)$, variance $\mathbf{u}$, and covariance Σ , coefficients $w_{forward}$, w_{left} , w_{right} denote the weights of the Kalman filter for each direction, and $w_{forward}$, w_{left} , w_{right} $=1$. From the results, we can calculate the distribution of the object by (7).

$$e_{expricit}(\mathbf{x},t) = \max\left\{p_t(\mathbf{x}), p_{t+1}(\mathbf{x}), \cdots, p_{t+N}(\mathbf{x})\right\} \quad (7)$$

2) Distribution prediction of the driver's car:

The position distribution of driver's car $\hat{x}_{Self}(t)$ is also calculated with the same procedure by (8), (9) and (10).

$$\hat{\mathbf{x}}_{Self}(t+1) \leftarrow \mathbf{F}_{Self}\hat{\mathbf{x}}_{Self}(t) \quad (8)$$

$$\hat{\Sigma}_{Self}(t+1) \leftarrow \mathbf{F}_{Self}\hat{\Sigma}_{Self}(t)\mathbf{F}_{Self}^{T}+\mathbf{G}\Sigma_w\mathbf{G}^T \quad (9)$$

$$p_{t+n}^{Self}(x) = \aleph\left(\hat{\mathbf{x}}_{Self}(t+n), \hat{\Sigma}_{Self}(t+n)\right) \quad (10)$$

Here, F_{Self} denotes a transition matrix based on the driver's action plan. By calculating the overlap of the position distributions along time, we get the predicted distribution of driver's car by (11).

$$e_{Self}(\mathbf{x},t) = \max\left\{p_t^{Self}(\mathbf{x}), p_{t+1}^{Self}(\mathbf{x}), \cdots, p_{t+N}^{Self}(\mathbf{x})\right\} \quad (11)$$

3) Calculation of predicted visible risky area:

We describe PVRA as $d_{explicit}(x,t)$. It is defin it as an overlap of predicted distribution $e_{explicit}(x)$ for the visible object and $e_{Self}(x)$ for the driver's car, it is calculated by (12).

$$d_{explicit}(x) = \min\left\{e_{explicit}(x,t), e_{Self}(x,t)\right\} \quad (12)$$

B. *Model of the Non-Visible Risky Area*

When we pass a blind intersection, we become aware of unseen cars that might emerge from the left or right blind corners. Such caution is based on a prediction that an unobservable car might approach from behind corners. In this paper, we call an area where a possibly oncoming car may collide with the driver's car the "Predicted Non-Visible Risky Area (PNRA)".

1) *Position estimation of the non-visible objects:*

In this study, we consider a case in which the driver's car is trying to go through an intersection (Fig. 3). We assume that a car coming from a blind corner collides with the driver's car at the center of intersectinon. The most probable scenario is that the car located at a distance D_c from the intersection center with average speed v_0 simulaneously arrive at the intersection with the driver's car ((a) in Fig. 3). The driver must always estimate the possible oncoming car's position and speed called D_c and v_0, respectively. We call the distance D_c *critical distance*, which is calculated by (13) where the driver's car's speed is denoted as v_s.

$$D_c / v_s = D_0 / v_0 \quad \Leftrightarrow \quad D_c = \frac{v_s}{v_0} D_0 \tag{13}$$

How does the *critical distance* changes when the driver's car approaches intersection and becomes visible from the occluded area behind the corner or object? The point D_0 is now observable and no car is found there. When we assume the speed of the oncoming car is distributed with average v_0 and decreasing probability along the deviation from the average, the most probable scenario is that the oncoming car is located at distance D_B in Fig. 3(b) where D_B is nearest to the intersection but still at an unobservable distance. In this case the probability of an oncoming car decreases because the car must travel faster than average to collide with the driver's car, and the probability of the speed is lower than that of v_0.

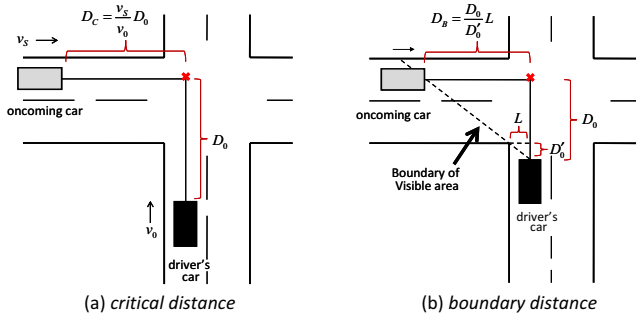

Figure 3. Prediction of non-visible object: (a) calculation of *critical distance*, (b) calculation of *boundary distance*.

Distance D_B can be calculated by (14) where θ is an angle from the front to observed the occluded corner (see Fig. 3 (b)), L is half of the road width and D_0 is the distance of the driver's car from the intersection. Distance D_B called the *boundary distance*.

$$D_B = D_0 \tan\theta = D_0 \frac{L}{D_0'} \tag{14}$$

Which distance of D_c and D_B should be choosen as an estimated distance of the oncoming car from the intersection? If $D_B < D_C$, the oncoming car must have slower speed to avoid collision with the driver's car. However the probability of slower speed is lower than that of the average speed, the oncoming car position at D_C should be had highest probability of collision. In contrast, the oncoming car must be observed from the driver's car when $D_B > D_C$. If the driver fail to observe the oncoming car, the driver must assume that the position of the coming car is at D_B.

2) *Distribution prediction of the non-visible objects:*

Based on the estimated position, the model predicts future position and distribution of the oncoming car using (15) and (16).

$$\hat{\mathbf{x}}_{implicit}(t+1) \leftarrow \mathbf{F}_{im} \hat{\mathbf{x}}_{implicit}(t) \tag{15}$$

$$\hat{\Sigma}_{implicit}(t+1) \leftarrow \mathbf{F}_{im} \hat{\Sigma}_{implicit}(t) \mathbf{F}_{im}^T + \mathbf{G} \Sigma_w \mathbf{G}^T \tag{16}$$

The initial value of $\hat{\mathbf{x}}_{implicit}(t_0)$ is set to the estimated position of the oncoming car. The matrix $\mathbf{F}_{im}$ originally represents a situation where the oncoming car enters the intersection at a speed to just collide with the driver's car. But this time, we used $\mathbf{F}_{im}$ with the fixed speed v_0 for simplicity. Then, the predicted distribution of the non-visible object is calculated by (17) and (18).

$$p_{t+n}^{implicit}(\mathbf{x}) = \aleph\left(\hat{\mathbf{x}}_{implicit}(t+n), \hat{\Sigma}_{implicit}(t+n)\right) \tag{17}$$

$$e_{implicit}(\mathbf{x}, t) = \max\left\{p_t^{implicit}(\mathbf{x}), p_{t+1}^{implicit}(\mathbf{x}), \cdots, p_{t+N}^{implicit}(\mathbf{x})\right\} \tag{18}$$

3) *Calculation of predictive non-visible risky area:*

With the calculation of non-visible object distribution along time, we can calculate the non-visible risky area (PNRA) for the blind corner as follows.

$$d_{implicit}(\mathbf{x}, t) = \min\left\{e_{implicit}(\mathbf{x}, t), e_{Self}(\mathbf{x}, t)\right\} \tag{19}$$

C. *Risk Evaluation and Eye Movement*

After calculating PVRA for observable objects and PNRA for non-visible objects, we can instantly compare the risk of the

environment and detect which object has the highest risk. We assume that the deriver is watching the object's current position that has the highest risk in the near future, but not the place of risk distribution. The object to be observed momentarily can be calculated as follows.

$$\mathbf{x}^* = \arg\max_{\mathbf{x}} \left\{ d_{explicit}(\mathbf{x},t), d_{implicit}(\mathbf{x},t) \right\} \qquad (20)$$

If the object is a non-visible, we assumed the driver can see from which direction the object can be seen first when it enters the visible area. Direction θ is calculated by (14).

III. EXPERIMENT

To verify the validity of our proposed model, we compared the reconstructed eye movements from our model with the actual eye movements of a driver on the road.

A. Recordings of Car Driver's Eye Movement

We recorded eye movements of a driving school instructor while he was driving on a predetermined course in a suburban area (around midoriyama housing estate in Machida city) of Tokyo. He wore an eye-mark recorder (EMR-8B, NAC) and drove a car (PRIUS, TOYOTA).

We selected a 240-m long cource (upper half of Fig. 4) on which the instructor drove from right to left at 34.3 km/h on average. There were eight intersections, a parked vehicle, and a pedestrian on the course, and the driver had to drive and pass the vehicle while predicting both risks. The line over the course indicates the gaze direction of the driver, upper-right and lower-left, along the course.

The lower part of Fig. 4 shows an example of a recorded driver's field of view and the gaze direction (white "+"), which we identified every 0.1 sec from the beginning of the course to the end.

Figure 4. Road map of actual driving experiment and measured direction of gaze (upper part) and a slice of eye movement data (lower part, eye direction indicated by white "+").

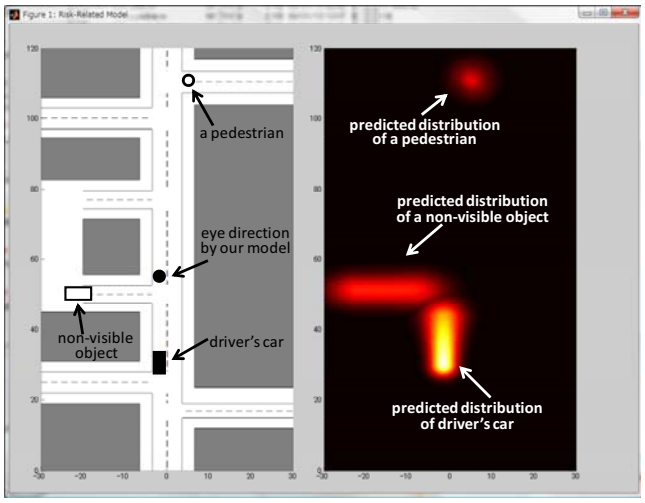

Figure 5. Example of predicted object distribution by the model. Left part shows a course map and right part shows predicted area of a non-visible object, a pedestrian, and driver's car.

B. Eye Movement Simulation

To evaluate the model, we prepared a 240-m driving computer simulation environment that resembled the test course and calculated eye direction with the same visual information as driver's using the proposed model. In the simulation experiment, the model predicted one second into the future in 0.05 sec steps and recalculated every 0.1sec step.

In the simulation, we divided the course into a former half area (120 m) and a latter half area (120 m), and considered an area around a bus stop at 180 m point from the start. The left side of Fig. 5 shows a birds-eye view of the latter half area, and the right side shows the predicted distribution of the objects and the driver's car by the model. In the left side of Fig. 5, the driver's car is indicated by a solid and black rectangle, a pedestrian is indicated by an open circle, a non-visible vehicle is indicated by a white rectangle, and the eye direction calculated by the model is indicated by a dot. In the right side of Fig. 5, the predicted distribution of the driver's car, the predicted distribution of the non-visible car, and a pedestrian are shown with ellipses. Places with lower probability are darkened, and ones with higher probability are brightened.

To evaluate the validity of our proposed model, we compared the reconstructed eye movements from our model with the actual eye movements of the driver on the test course. To quantify the similarity of the reconstructed eye movements with the actual eye movements, we identified driver's eye directions and the objets toward driver's eye direction every 10 m (block) on the test course and compared them. Table 1 shows the gaze direction of the driverr and our proposed model at each block on the test course. Symbols "F", "L", "R", "M", and "P" mean "forward direction", "left side", "right side", "side mirror", and "parked vehicle" respectively.

TABLE I. EYE DIRECTION COMPARISON BETWEEN ACTUAL DRIVER'S AND MODEL.

Eye Direction	Blocks									
	1	2	3	4	5	6	7	8	9	10
Actual Driver	F	M	L	F	P	P	P	F	R	F
Model	F	L	L	F	R	R	R	F	R	L

Eye Direction	Blocks								
	11	12	13	14	15	16	17	18	19
Actual Driver	F	M	L	F	P	P	P	F	R
Model	F	L	L	F	R	R	R	F	R

F: Forward direction, L: Left side, R: Right side, M: Side mirror, P: Parked vehicle.

Our proposed model successfully reconstructed 73.6% of the driver's actual eye movements. On the other hand, the model failed to reconstruct the eye movements of side mirror (Table1 2nd and 12th blocks.) This is only because the model does not support the side mirror object. Moveover, the model also failed to construct the eye movement of the narrow intersections (Table 1: 5th, 6th, and 7th blocks). There are two interpretations on this result. The first one is that these intersections probably should have been observed, but the driver missed them. Such human error attending the visible risk overrides the non-visible risk. The second one is that the driver knows that there are less risk in these intersections, where moving objects are raely appeared normally.

If we assume that the latter case is correct, the accuracy will be improved by indroducting the prior knowledge about the intersections. Meanwhile, if we assume that the first case is correct,our system should support dirvers if it can detect such human error and only gives alerts when the error is caused without any other reason. We need more precise driver's models to determine if error alerts should be issued.

IV. CONCLUSION

In this paper, we proposed a computational model for eye movements while driving a car. In our model, the probability distributions of the surrounding objects' existence and the probability distribution of a driver's car position were calculated by predicting the behavior of objects using Kalman filters and prior probability distributions. Two types of risky area, PVRA and PNRA were calculated using these probability distributions. Drivers moved their eyes toward the risky objects to obtain more precise information for the prediction.

In addition, we compared the reconstructed eye movements of the model and the actual eye movements of the drivers while driving on a road. Our model could explain the eye movements for PVRA and PNRA, but it could not reconstruct the actual eye movements such as neglecting narrow intersections due to human error or some other reasonable mechanism. Human drivers might have rules or prior knowledge about ordinary traffic that they might apply to the actual decision making for driving. We plan to improve our model to inhibit redundant eye movements and to overcome the above drawbacks, and evaluate the model by increased number of subjects behavior. We believe that if the model is successfully improved and the environments, which are the intersections, other cars and so on, are correctly recognized automatically, we can get stressfree safety driving system.

REFERENCES

[1] K. Mizutani, G. Saito, T. Omori, and A. Ogawa, "A feasibility study of cognitive computation model for driver's process estimation from driving behavior," IEICE technical report. Neurocomputing, vol. 103, pp. 25-30, 2004.

[2] K. Mizutani and T. Omori, "A feasibility study of driver's cognitive process estimation from driving behavior," IEEJ Trans. EIS, vol. 125, pp. 967-975, 2005.

[3] Y. Togashi, T. Omori, and K. Yamauchi, "Model of driver eye motion based on driving plan and prediction of changes in the environment," Proc. of the 2007 IEEE Symposium on Foundations of Computational Intelligence, pp. 289–295, 2007.

[4] T. Al-Shihabi and R. Mourant, "A framework for modeling human-like driving behavior for autonomous vehicles in driving simulators," Proc. The Fifth International Conference on Autonomous Agents, pp. 286–291, 2001.

[5] D. D. Salvucci, "Modeling driver behaviro in a cognitive architecture," Human Factors, vol. 48, pp. 362–380, 2006.

[6] D. D. Salvucci, H. M. Mandalia, N. Kuge, and T. Yamamura, "Lane-change detection using a computational driver model," Human Factors, vol. 49, pp. 532–542, 2007.

[7] M. Sato, Y. Togashi, T. Omori, K. Yamauchi, S. Ishikawa, and T. Wakita, "Computational modeling of risk-related eye movement of car drivers," Proc. International Conference on Neural Information Processing, in press.

[8] N. Sprague and D. Ballard, "Eye movements for reward maximization,"Advances in Neural Information Processing Systems vol. 16, pp. 1467-1474, 2004.

[9] R. E. Kalman, "A new approach to linear filtering and prediction problem," Journal of Basic Engineering, 82D, pp. 34–45, 1960.